JPRS-UMS-90-004
31 AUGUST 1990

FOREIGN BROADCAST INFORMATION SERVICE

JPRS Report

Science & Technology

USSR: Materials Science

JPRS-UMS-90-004
31 AUGUST 1990

SCIENCE & TECHNOLOGY

USSR: MATERIALS SCIENCE

CONTENTS

UDC 669.14.018.8

Corrosion Cracking of Steels 03Kh20N18M2D2, 06KhN28MDT Under Effect of Plastic Deformation

907D0140A Tbilisi SOOBSHCHENIYA AKADEMII NAUK GRUZINSKOY SSR in Russian
Vol 136 No 2, Nov 89 (manuscript received 31 Mar 89) pp 393-395

[Article by G. Sh. Kobulashvili and L. F. Tavadze, Metallurgy Institute im. 50th Anniversary of the USSR at the Georgian Academy of Sciences; submitted by Academician F. N. Tavadze]

[Text] In developing structural materials intended for manufacturing production equipment which operates in corrosive media, one must establish steel's tendency to such dangerous types of corrosion as intercrystalline, pitting, and stress corrosion in addition to examining its corrosion resistance.

In the present paper we examine the propensity of chrome–nickel austenite steel 03Kh20N18M2D2 to corrosion cracking; this steel was developed for fluorine– and sulfuric acid-containing highly corrosive media to replace high–alloy acid resisting steel 06KhN28MDT [1]. In order to estimate the corrosive failure of the new steel under plastic straining in a 42% $MgCl_2$ solution, alloy 06KhN28MDT was also tested at the same time.

These steels' tendency to corrosion cracking was determined using the most rigid method – tests at a constant straining rate [2] where the sample's straining rate is one of the principal parameters affecting corrosion cracking.

Tests were carried out at a constant straining rate in AIMA–5–2 testers intended for long–term strength and creep tests. In order to expand the sample straining rate range, special reduction systems were developed for AIMA–5–2 testers; these systems made it possible to vary the active grip travel speed within a broad range from 10^{-6} to 10^{-9} m/s.

In order to conduct the tests under conditions which reproduce equipment operating conditions in high–temperature chloride–containing media, special chambers were developed, making it possible to conduct tests in a 42% $MgCl_2$ solution at 154°C. The strain diagrams (load/elongation) were recorded during the tests. The results of comparative tests

of steels 06KhN28MDT and 03Kh20N18M2D2 to examine their tendency to corrosion cracking at a constant straining rate are summarized in the table.

The Tendency of Steels 06KhN28MDT and 03Kh20N18M2D2 to Corrosion Cracking in a 42% $MgCl_2$ solution at 154°C at a Constant Deformation Rate

Brand of steel	Straining rate, s^{-1}	Test results					
		P_{max}, kg	σ_{max}, kg/mm²	ε_p	δ, %	a_p*, mm	τ, h
03Kh20N18M2D2	$1.6 \cdot 10^{-5}$	840	42	9.2	37	0.35	10
	$5.5 \cdot 10^{-5}$	800	40	8.0	32	0.20	16
	$1.6 \cdot 10^{-6}$	750	37	5.6	22	0.44	38
	$5.5 \cdot 10^{-6}$	760	38	5.3	21	0.31	107
06KhN28MDT	$5.5 \cdot 10^{-5}$	1,180	59	10.5	42	0.21	22
	$1.6 \cdot 10^{-6}$	1,140	57	7.4	30	0.32	50
	$5.5 \cdot 10^{-6}$	1,000	50	7.0	28	0.25	87

*The crack length was measured under a metallographic microscope

For a metal/medium system in which the product's service life is primarily determined by the macrocrack growth stage, we suggest that the methods of fracture mechanics be used in strength and durability analyses employing the relationships derived in [3] where the fracture parameters were colligated with the straining rate with the help of empirical coefficients:

$$\tau_p = Z\dot{\varepsilon}^{-\frac{n+1}{M}},$$

$$\varepsilon_p = Z\dot{\varepsilon}^{-\frac{m}{M}},$$

$$a_p = KZ^m\dot{\varepsilon}^{-\frac{m}{M}(n+1)},$$

$$V_p = KZ^{m-1}\dot{\varepsilon}^{\frac{(1-m)(n+1)}{m}},$$

where τ_p is the time to failure; ε_p is elongation at the moment of fracture; a_p is the crack length at the moment of fracture; V_p is the mean crack propagation velocity; and m, n, G, K are the coefficients determined experimentally which make it possible to determine M and Z.

$$M = m + n + 1, \quad Z = \left(\frac{G}{M}\right)^{\frac{1}{M}}.$$

The aforementioned equations embedded in a computer (EVM) program make it possible to calculate the mean crack propagation rate at equal metal straining rates.

In particular, the above computation shows that given the most optimal straining rate of $1.6 \cdot 10^{-6}$ s^{-1}, the corrosion crack propagation rate for steels 03Kh20N18M2D2 and 06KhN-28MDT under study amounts to $3.7 \cdot 10^{-6}$ and $1.6 \cdot 10^{-6}$ mm/s, respectively.

Thus, with respect to corrosion cracking resistance characteristics in a 42% $MgCl_2$ solution at 154°C, the steels under study are close to, or exceed, steels 10Kh17N13M2T and 08Kh18N10T whose corrosion crack propagation rate under similar testing conditions at $\varepsilon = 1.1 \cdot 10$ s^{-1} is equal to $8.2 \cdot 10^{-5}$ and $4.46 \cdot 10^{-5}$ mm/s, respectively. Consequently, the new brand of steel can be recommended for manufacturing equipment which operates in highly corrosive fluorine and sulfuric acid-containing media.

Bibliography

1. V. S. Zotikov, G. Sh. Kobulashvili, E. Ya. Semenyuk, V. A. Gerasimova. "Tezisy dokladov Vsesoyuznoy n/t konferentsii "Progressivnyye metody i sredstva zashchity metallov izdeliy ot korrozii"" [Proceedings of the All-Union Scientific and Engineering Conference on Advanced Methods and Means of Protecting Metal Products From Corrosion]. Vol. II, Moscow, 1988.

2. R. N. Parkins, R. G. Matsts, Zh. Zh. Roysl, Zh. K. Skalli [as transliterated]. ZA-ShchITA METALLOV, vol. IX, No. 5, 1973.

3. A. A. Nazarov. SUDOSTROITELNAYa PROMYShLENNOST: SERIYA METALLOVEDENIYe, No. 3, 1986.

UDC 669.187.526.001.5

Properties of High-Cleanness High-Strength Steel 12GN2MFAYu

907D0112A Kiev PROBLEMY SPETSIALNOY ELEKTROMETALLURGII in Russian No 1, Jan-Mar 90 pp 99-106

[Article by L. I. Mikhoduy, M. B. Movchan, V. D. Poznyakov, G. N. Strizhius, Electric Welding Institute im. Ye. O. Paton, Kiev: "Properties of High-Cleanness High-Strength Steel 12GN2MFAYu"]

[Text] Because of the rapid development of extensive regions with low climatic temperatures in this country the use of steels with increased cold resistance in the welded metal structures of powerful mining equipment is now becoming an urgent problem. To produce these steels metallurgical enterprises use electroslag remelting (ESR), argon blasting, and synthetic slag processing[1,2] or other measures that effectively remove harmful impurities from the metal. However, recent works devoted to the weldability of these steels disagree on the influence of the metal's cleanness on the resistance of welded joints to cold crack formation.

For example, references 3, 4 and others state that the likelihood that a crack will form in the heat-affected zone (HAZ) of alloyed steels increases if the sulfur content is reduced to 0.001 percent. The authors of references 5-7 came to the conclusion that a change in the sulfur content in low-alloyed steels from 0.001 to 0.02 percent has a negligible effect on their sensitivity to crack formation. Reference 8 explains the discrepancy in the results from different authors by the effect that steel composition and the kind of nonmetal inclusions (NI) have on structure formation and properties of the HAZ in welded joints of high-cleanness steel.

The objective of this article is to study the effect of the amount of harmful impurities on the resistance of high strength steel 12GN2MFAYu (VS-1) to delayed and brittle failure.

Open hearth steel VS-1 without additional refining (control specimens) and after argon blasting (VS-1-U) and electroslag remelting (steel VS-1-Sh) was selected for this research.

Table 1 shows the chemical composition of these steels, as well as the content of basic impurities. A comparison of the data in this table shows that the

these steels differ basically in sulfur content, the limit quantity of which varied from 0.009 to 0.032 percent.

The effect of steel 12GN2MFAYu's cleanness in terms of basic impurities on the properties of its welded joints was studied by metallographic analysis of 20-mm-thick specimens of this steel, including measurement of hardness, a quantitative study of the type, morphology, and size of the NI, and study of the microstructure and the structure of the austenite grain of these specimens.

Table 1

Element	Steel grade		
	VS-2	VS-1-U	VS-1-Sh
	Mass fraction of elements, percent		
C	0.15	0.139	0.125
Si	0.41	0.34	0.28
Mn	1.14	1.12	1.06
Cr	0.38	0.53	0.52
Ni	1.56	1.64	1.58
Mo	0.22	0.21	0.2
Cu	0.19	0.22	0.21
V	0.07	0.09	0.087
Al	0.06	0.09	0.05
N_2	0.018	0.027	0.027
S	0.032	0.013	0.009
P	0.014	0.011	0.011
	Gas content, percent		
[O]	0.024	0.026	0.00002
[N]	0.025	0.0272	0.00002
[H]	0.028	0.0277	0.00002

Measurement of the hardness (HV) of steel VS-1, VS-1-U, and VS-1-Sh specimens showed that VS-1-U has the highest (HV 250-265), while VS-1 has the lowest (HV 220-240). Steel specimens after ESR were in between (HV 240-257).

Metallographic study of the type and morphology of NI was performed on a "Neofot-3" metallographic microscope by visual inspection of polished unetched specimens. The quantity and distribution of NI were determined by "L" linear method (GOST 1778-70). The results were used to plot curves relating the quantity of inclusions (contamination index) I_i to their size.

The average size of the inclusions d_{av} in all morphological groups was determined by the method described in reference 9. Table 2 gives the values for d_{av}.

It was established that the NI in all steel specimens were primarily sulfides, oxides, oxysulfides, silicates, and nitrides. However, the ratio of the

amount of inclusions in these morphological groups, the sizes of the inclusions, and their total quantity differed sharply in the open hearth steels and those that had been refined (table 2, fig. 1).

Table 2

Steel grade	Average inclusion size and degree of metal contamination										$I_{tot} \times 10^3$	D_g, μ
	Sulfides		Oxides		Oxysulfides		Silicates		Nitrides			
	d_{av}, μ	$i_c \times 10^3$	d_{av}, μ	$i_o \times 10^3$	d_{av}, μ	$i_{os} \times 10^3$	d_{av}, μ	$i_{sil} \times 10^3$	d_{av}, μ	$i_n \times 10^3$		
VS-1	18.1	3.1	6.65	1.4	8.49	1.0	7.19	1.05	4.88	1.55	8.1	26.8
VS-1-U	5.49	1.6	4.19	1.7	4.99	1.0	3.29	1.1	3.5	1.65	7.05	16.6
VS-1-Sh	6.25	1.3	6.87	1.2	8.0	0.90	6.35	1.1	7.02	1.6	6.1	89.42

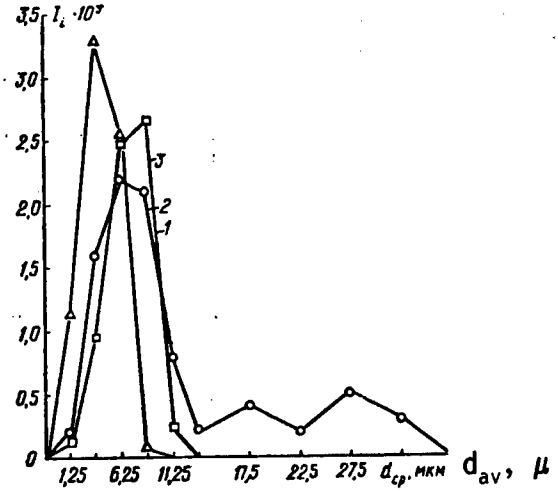

Fig. 1. Distribution of the total contamination index for steels VS-1 (1), VS-1-U (2), and VS-1-Sh (3) by nonmetal inclusions as a function of their size.

The open hearth steel contains elongated (to 37.5 μ) iron-manganese sulfides, a large quantity of acute-angled silicate inclusions, and comparatively large (to 13.5 μ) oxide and (to 11.5 μ) nitride inclusions. The total contamination index for this steel is $I_{tot}=8.1 \times 10^3$.

Quantitative metallographic studies of the NI showed that refining steel 12GN2MFAYu decreases the total contamination index to 7.05×10^3 in specimens of steel VS-1-U and to 6.1×10^3 in specimens of steel VS-1-Sh. This is accompanied by a narrowing of the size range of the distribution of all types of inclusions and a reduction in the average size of inclusions in all morphological groups.

A study of the microstructure of these variations of steel 12GN2MFAYu exposed in a 4-percent alcohol solution of HNO_3 was performed on a "Neofot-2" metallographic microscope. Check measurements of microhardness were done with a PMT-3 micro-hardness gauge at a load of 50 g. Figure 2 shows the bainite-martensite microstructure typical for specimens of this steel.

Caption: Figure 2. Microstructure (200X, red. 3/4) of steels VS-1 (a), VS-1-U (2), and VS-1-Sh (c). [not reproduced].

Quantitative metallographic analysis of the austenite grain structure was performed on polished specimens of steels VS-1, VS-1-U, and VS-1-Sh after vacuum thermal etching at 1100°C for 1 hr. Grain size D_g and average inclusion size were determined by the procedure detailed in reference 9.

Figure 3 shows that specimens of steel VS-1-Sh have the largest grain, 300 μ, while it does not exceed 100 μ in specimens of steel VS-1 and VS-1-U. The most typical grain size, corresponding to the maximum on the grain size distribution frequency curve is: minimum, 18 μ, in specimens of steel VS-1 processed with argon; maximum, 60 μ, in specimens of steel VS-1-Sh; intermediate, 30 μ, in specimens of open hearth steel. In addition, specimens of VS-1 and VS-1-U are distinguished by more uniform grain size distribution than are specimens of VS-1-Sh, i.e., steel VS-1-Sh has greater grain variety.

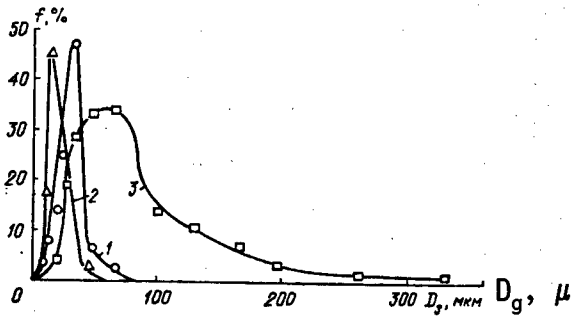

Figure 3. Austenite grain size frequency distribution for steels VS-1 (1), VS-1-U (2), and VS-1-Sh (3).

The following tests were performed to evaluate the effect that refining steel 12GN2MFAYu has on its cold resistance: tension tests on cylindrical specimens 10 mm in diameter, Mesnager and Charpy impact bending tests at temperature to -70°C on notched specimens 10 x 10 mm in cross section, and tests on specimens measuring 320 x 320 x 20 mm by the procedure described in reference 10.

It was established that as test temperature drops, the indicators of strength and resistance to macroplastic strain in all three versions of steel 12GN2MFAYu increase monotonically (fig. 4), while ductility indicators remain almost unchanged. This indicates their rather high serviceability in the absence of stress concentrations under static loading at temperatures to -60°C.

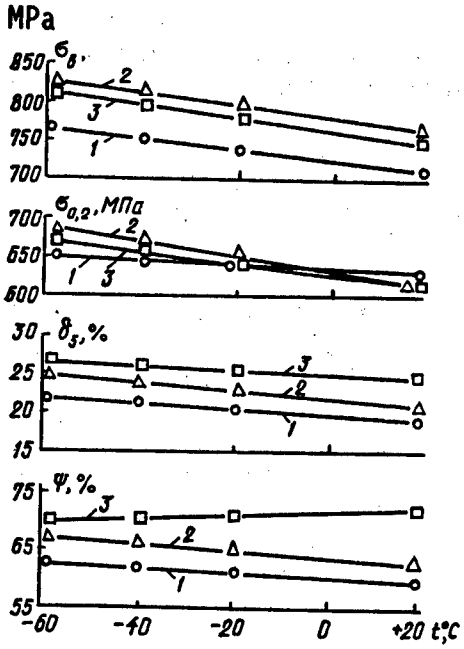

Figure 4. Temperature profiles for the strength and ductility of steels VS-1 (1), VS-1-U (2), and VS-1-Sh (3).

Figure 5. Temperature profile of the failure viscosity of steels VS-1 (1), VS-1-U (2), and VS-1-Sh (3) during impact bending (F_B=percentage of fiber in the fracture.

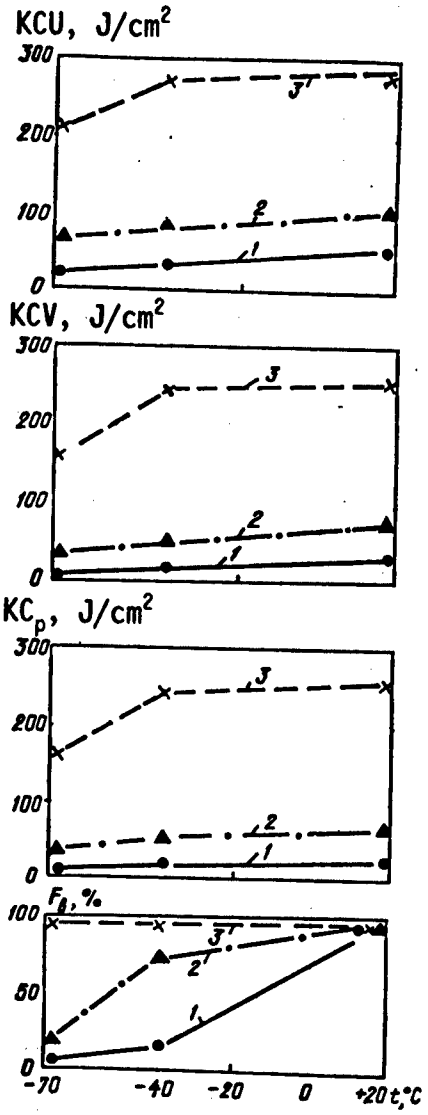

The results of impact strength tests confirm this situation. Figure 5 presents the temperature profiles for impact strength, which show that at -70°C impact strength KCU of steel VS-1 exceeds 30 J/cm^2, while that of steels VS-1-U and VS-1-Sh is 70 and 200 J/cm^2.

Critical brittleness temperature at KCV≥29 J/cm^2 is -10°C in steel VS-1. The steel is distinguished by inadequate resistance to brittle and viscous failure, and at the temperatures studied crack propagation effort KC_p is 5-25 J/cm^2, while crack origination effort KC_3 is 20-30 J/cm^2.

The critical brittleness temperature of steels VS-1-U and VS-1-Sh is below -10°C; crack origination effort is 30-40 J/cm^2. Crack propagation effort in the steel processed with argon increased significantly and was 27-67 J/cm^2. However, the steel 12GN2MFAYu that had undergone electroslag remelting had the highest indicators for resistance to brittle failure.

Fractographic studies showed that fractures in specimens of steel VS-1 have a significant quantity of string inclusions along the rolling lines (fig. 6, a).

Argon processing shortens the strings and reduces their size and number (fig. 6, b). Inclusions in steel 12GN2MFAYu after ESR have a globular shape, and there is no separation in the fracture. The matrix undergoes viscous failure (fig. 6, c).

Caption: Figure 6. Fractures in specimens of steels VS-1 (a), VS-1-U (b), and VS-1-Sh (c) after impact bending tests at 20°C (10X, red. 3/4).

Specimens measuring 320 x 320 x 20 mm were tested to evaluate the effect of stress concentration, full cross section size, and the high strain rate on the change in strength and viscosity characteristics. The specimens were loaded with tensile loads. Loaded specimens were cooled at the notch with liquid nitrogen using clamp-on tanks. Failure was initiated by an impact along a steel insert in the notch. The cracks that developed at the end of the notch spread across the specimen's width and, depending on load, temperature, and steel viscosity, stopped or crossed the entire specimen. The metal's temperature at the end of the crack, critical crack arrest temperature t_{ca}, was calculated with the viscosity indicator; the specimen tensile stress corresponding to this temperature, by the critical crack arrest stress σ_{cs}.

Test results (fig. 7) show that steels VS-1-U and VS-1-Sh at temperatures to -70°C can effectively retard a moving crack at nominal tensile failure stresses no higher than 250 MPa. VS-1 is far inferior to them in terms of this indicator. At a similar σ_{cs}, its critical crack arrest temperature is very high.

The results of these studies show that low-carbon martensite-bainite steel 12GN2MFAYu after refining (ESR and argon blasting) has high cold resistance indicators at temperatures to -70°C. The basic task in welding these steels consists in preventing the formation of cold cracks in the joint and producing a sufficiently viscous HAZ metal. For open hearth steel 12GN2MFAYu this problem was solved by using welding conditions[11] which ensure a range of cooling rates of W_{cl}=3.0-17.0°C (at temperatures of 600-500°C) with a diffusive hydrogen content $[H]_{dif}$ in the weld metal no higher than 4.0-4.5 ml/100 g (from results of chromatographic analysis).

The resistance of the HAZ metal in these steels to the formation of cold cracks was evaluated by implant method. Insert specimens 6.0 mm in diameter with a stress concentrator in the form of a spiral groove with a pitch of 2.0 mm and a radius of 0.1 mm were tested. The specimens installed in holes in a 20-mm-thick base plate firmly secured in the test setup were welded in one pass with an ANP-2 electrode 4.0 mm in diameter at I_w=170 A, U_a=25 V, v_w=8 m/hr. Welded joint cooling rate (W_{col}=19 and 17°C/sec) was varied by changing the initial temperature of the plate. The amount of diffusive hydrogen ($[H]_{dif}$=3.8, 7.0, and 13.0 ml/100 g) was determined by chromatography. Specimen loading began during post-welding cooling to 120-100°C.

Figure 8 presents values for critical tensile stresses σ_{kp} in implant specimens of steels VS-1, VS-1-U, and VS-1-Sh when welded joint cooling rate and the content of diffusive hydrogen in the welds are varied. At slow cooling rates (W_{col}=10°C/sec) with a limited hydrogen content ($[H]_{dif}$=3.0 ml/100 g) these steels have a sufficiently high resistance to delayed failure.

If the welded joint cooling rate is increased and their hydrogen content is simultaneously increased to 7.0-13.0 ml/100 g, all three modifications of steel 12GN2MFAYu have a strong tendency to delayed failure (fig. 8, b). This pertains particularly to highly clean steels that have been refined.

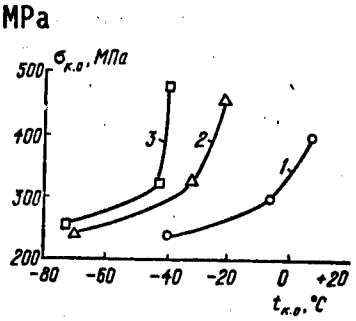

Figure 7. Critical stresses from the delay in brittle failure in impact crack initiation and tension in specimens of steel VS-1 (1), VS-1-U (2), and VS-1-Sh (3) related to test temperature.

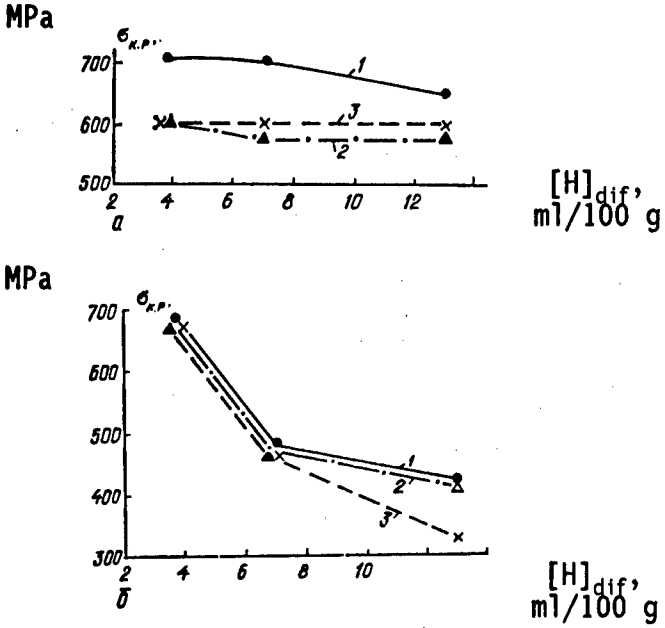

Figure 8. Effect of hydrogen content in a welded joint on critical tensile stress in implant specimens of steels VS-1 (1), VS-1-U (2), and VS-1-Sh (3): a - W_{col}=10°C/sec; b - W_{col}=10°C/sec.

This is probably because loose multiphase oxysulfide nonmetal inclusions in the steel delay hydrogen diffusion and its entry to the zone of local plastic strain at the apex of the developing crack[12]. Therefore if the hydrogen content is high enough ($[H]_{dif} \geq 7.3$ ml/(100 g), its concentration at the apex of a crack in steel VS-1 with a large amount of NI ($I_{tot}=8.1 \times 10^3$) is much lower than in steels VS-1-I ($I_{tot}=7.05 \times 10^3$) and VS-1-Sh ($I_{tot}=6.9 \times 10^3$) with a small amount of NI.

These studies indicate that if basic requirements for the process of welding high strength steels are met (using optimum welding conditions and limiting the hydrogen content in the welds to $[H]_{dif} \leq 4.0$-4.5 ml/100 g), welded joints of highly clean steel 12GN2MFAYu are distinguished by high resistance to delayed failure.

Conclusions

1. Refining steel 12GN2MFAYu by electroslag remelting and blasting the metal with argon promotes a beneficial ratio among typical NI morphological groups: a reduction in the specific percentage of sulfides, oxides, and silicates and an increase in the specific percentage of oxysulfides. This narrows the range of inclusion size distribution.

2. Increasing the cleanness of steel 12GN2MFAYu by argon blasting shifts the maximum on the austenite grain size distribution frequency curve toward lower values, i.e. it helps increase austenite grain structure uniformity.

3. The change in the quantity of NI and the austenite grain structure increase the ductility and impact strength of steel 12GN2MFAYu after refining.

4. Reducing the overall contamination by nonmetal inclusions makes it possible to increase the cold resistance of high-strength steel 12GN2MFAYu used in static and impact loading at a temperature to -70°C.

5. An increase in the content of diffusive hydrogen because of its localization in the discontinuities in loose multiphase oxysulfide inclusions and an increase in the welded joint cooling rate above permissible levels help increase the tendency of the HAZ metal in highly clean high-strength steel 12GN2MFAYu to delayed failure.

References

1. B. Ye. Paton, B. I. Medovar, V. A. Tikhonova, et al., "Study of the Possibility of Increasing the Quality of Plate Structures of High-Strength Structural Steel 12GN2MFAYu (VS-1) and 12KhGN2MFBAYu (VS-2) by Electroslag Remelting," PROBL. SPETS. ELEKTROMETALLURGII, 1984, No. 21, pp. 3-7.

2. B. Ye. Paton, B. I. Medovar, V. A. Tikhonova, et al., "Electroslag Remelting of High-Strength Structural Steel 12GN2MFAYu (VS-1) under Fluxes Containing REM Compounds," PROBL. SPETS. ELEKTROMETALLURGII, 1985, No. 1, pp. 5-7.

3. Y. Hirai, S. Minakami, J. Tsuboi, "Effects of Sulfur on Hydrogen-Assisted HAZ Cracking in Al-Killed Steel Plates," IIW, Doc. IX-1160-80.

4. P. H. M. Hart, "The Influence of Steel Cleanness on HAZ Hydrogen Cracking: The Present Position," IIW Doc. IX-1308-84.

5. H. Suzuki, "Weldability of Modern Structural Steels," Houdremont Lecture, 1982, 28 pp.

6. N. Serio, T. Saito, H. Miyasaka, "Effect of Sulfur and Nitrogen on Cold Cracking," MONTHLY REP. NSC, Apr. 1981, pp. 9-10.

7. N. Yurioka, S. Ohshita, T. Saito, "Effect of Sulfur on Cold Cracking," Ibid,m Aug. 1981, pp. 33-34.

8. M. Okumura, T. Kasuya, N. Yurioka, K. Nagano, "Effect of Cleanness of Steel on its Weldability," QUARTERLY J. JAP. WELD. SOC., 1988, vol. 6, No. 1, pp. 144-150.

9. V. F. Musiyachenko, I. S. Melnik, V. M. Kiryakov, "Effect of Modification of Nonmetal Inclusions by Rare-Earth Metals on the Structure and Properties of Weld Metal During Welding of High-Strength Steel," AVTOMAT. SVARKA, 1987, No. 6, pp. 1-6.

10. B. S. Kasatkin, V. F. Tereshchenko, G. N. Strizhius, Ye. V. Martsenko, "Cold Resistance of Welded Joints of High-Strength Steel 12GN2MFAYu," Ibid., 1982, No. 2, pp. 38-42.

11. V. F. Musiyachenko, B. S. Kasatkin, L. I. Mikhoduy, S. L. Zhdanov, "Welding High-Strength Steel 12GN2MFAYu," Ibid., 1982, No. 5, pp. 47-50.

12. Y. Kikuta, T. Araki, A. Hirose, N. Matsuda, "Effect of Nonmetallic Inclusions on Weld Cracking," QUARTERLY J. JAP. WELD. SOC., 1985, vol. 3, No. 3, pp. 137-143.

UDC 69.14.018.252.3

Microfractographic Study of High-Speed Steel Produced from Powder

18420207A Moscow IZVESTIYA AKADEMII NAUK SSSR: SERIYA METALLY No 2, in Russian Mar-Apr 89 (Manuscript received 28 Mar 88) pp 129-33

[Article by I. K. Kupalova, Ye. P. Kalinushkin, V. L. Shtark, Moscow]

[Text] At the present time, in connection with the development of robot engineering and flexible production systems, the most important requirement placed on a tool has come to be its operational reliability. As experience has shown, tools frequently fail due to chipping, microscopic cracking, and breaking of cutting elements following slight wear.[1]

Basic strength studies[2] have shown that in real material stress concentrators are always present (notches or edges of cracks), formed in the process of mechanical and (or) heat treatment, or arising during use. Therefore, one factor determining the serviceability and operational reliability of products, in addition to the resistance to the development of cracks, is resistance to their propagation, i.e., the ability to survive after a crack has started.[3-5]

According to some predictions, the production and consumption of parts of powder steel will expand. Therefore, determination of the possibility of achieving good operational reliability and methods of its improvement (from the standpoint of material structure) for tools made of high-speed steel powder is a practically important problem of today.

We have, therefore, undertaken a comparative investigation of the microstructure of fractures, i.e., the nature of propagation of cracks, in impact testing of unnotched specimens of high-speed type R6M5F3-MP powder steel and high-speed steel type R6M5-OMSP produced by the usual metallurgical method (Footnote 1: The chemical composition of the steels studied is quite similar: R6M5F3-MP and R6M5-OMSP contain, mass %: W 6.2 and 6.1, Mo 5.7 and 5.2, V 3.4 and 2.0, Cr 4.0 and 4.1, C 1.3 and 0.7.) after hardening from 1190-1280°C and optimal tempering at 560°C, 3 times of 1 hour each, on a type ZSM-35 scanning electron microscope manufactured by the Japanese "JEOL" company, with construction of the image of secondary electrons with an accelerating voltage of 25 kV and goniometer angle 45° by examination of 20 fields in each specimen (fracture) and subsequent averaging of the parameters investigated (Footnote 2: Information on type of fracture—parameters A, B, C, D, S (cf. Figure 1) was added in memory on an HP-97 (USA) calculator using a special program

(written in HPL language). With confidence probability 95%, the confidence intervals are: ΔA—1%, ΔB—2.5, ΔC, ΔD—2.0%, ΔS, Δd—0.3 μm, ΔKC—0.02 MJ/m^2; σ_{bnd}—250 MPa.). The quantitative microfractographic results thus obtained were compared with the austenite grain size, bending strength and impact toughness of these steels, as well as the life testing of milling cutters.

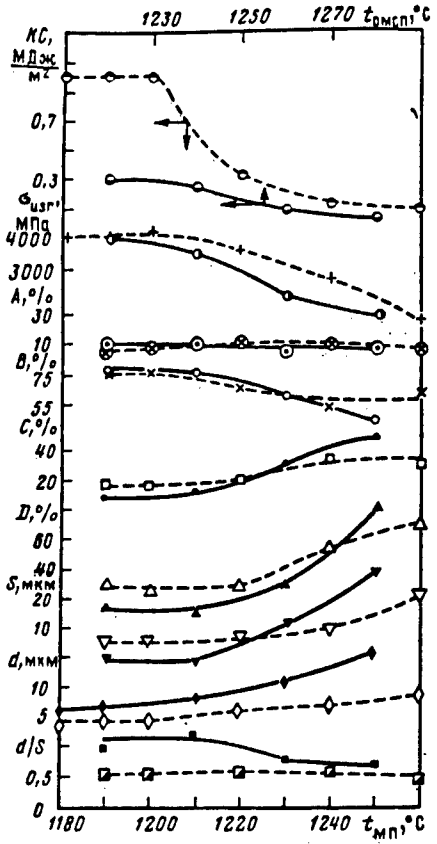

Figure 1. Change in Impact Toughness (KC), Bending Strength (σ_{bnd}) and Percent of Viscous Fracture (A), Viscous Chipping (B), Brittle Fracture (C), Intercrystalline Fracture (D) and Size of Facets of Intercrystalline Fracture (S), Size of Austenite Grain (d) and Their Ratio d/s as a Function of Hardening Temperature for Steel Types R6M5-OMSP (Solid Lines) and R6M5F3-MP (Dash Lines) After Optimal Tempering

The results obtained are presented in Figures 1-4, analysis of which indicates that the bending strength of these steels actually differs little up to a hardening temperature of 1200°C for R6M5F3-MP steel, 1240°C for R6M5-OMSP steel. As the hardening temperatures increase beyond these levels, the bending strength of R6M5-OMSP steel is lower than that of R6M5F3-MP steel. Throughout the entire hardening temperature interval studied, the impact toughness of R6M5-OMSP was lower, the austenite grain size was larger, than R6M5F3-MP. The percentage of viscous fracture area in the two steels was virtually identical. At hardening temperature up to 1230°C for R6M5-OMSP and 1200°C for R6M5F3-MP, the latter steel showed some tendency toward a higher percentage of brittle and intergrain fracture, as well as somewhat larger facet size (Footnote 3:

That surface of the fracture formed by failure along the boundaries of one austenite grain.) of intergrain fracture. Due to the smaller austenite grain by a factor of about 2 in the powder steel, coefficient K (ratio of austenite grain size to size of intergrain fracture facets) was also less.

Detailed comparative analysis of fractures after hardening from temperatures of up to 1230°C for R6M5-OMSP steel and up to 1200°C for R6M5F3-MP steel with optimal tempering showed that in the former steel, in addition to the greater dispersion of cup fracture, there is considerable fiber content, anisotropy or textured fracture, rough banding, whereas in R6M5F3-MP steel equiaxial fracture is observed (cf. Figures 2 and 3). As the hardening temperature rises to about 1230°C for R6M5-OMSP and 1200°C for R6M5F3-MP steel, there is an increase in both steels in areas with brittle fracture with a decrease in the number of sections of viscous fracture and an increase in the percentage and size of intergrain fracture facets. In R6M5-OMSP steel, we frequently see clear intergrain fracture with precise delimitation of boundaries, while the grains themselves fracture either by viscous or mixed viscous-brittle mechanisms; many dispersed particles are seen at these boundaries, with many cracks between individual boundaries.

One peculiarity of the structure of R6M5F3-MP powder steel after hardening from over 1200°C is that there are sections with large quantities of nonmetallic inclusions, as well as cracking with delamination, and lamellations, which may consist of nonmetallic inclusions. Throughout the entire hardening temperature range studied, an approximately constant value of coefficient K is retained for the powder steel, whereas in R6M5-OMSP steel, hardened at over 1260°C, its value decreases.

However, at all hardening temperatures in R6M5F3-FP steel, coefficient K is approximately half its value in R6M5-OMSP steel. According to many researchers,[2-5] the energy consumption of crack propagation is higher, the greater the value of K. Consequently, based on the results of our study, in type R6M5F3-MP powder steel with lower value of K, the crack propagation energy consumption, i.e., the energy necessary for fracture, is lower throughout the entire interval of hardening temperatures studied: fracture is easier than in R6M5-OMSP steel. These studies agree with reference 6, at which a comparative study of steels 10R6M5K5-OMSP and R6M5K5-MP showed (for hardening from 1210°C and tempering at 550°C, 3 times of 1 hour each) that the powder steel, with higher bending strength and impact toughness, had lower fracture toughness K_{Ic} in comparison to steel produced by ordinary metallurgical methods.

Thus, high-speed powder steels are superior to high-speed ordinary steels in crack formation resistance but inferior in crack propagation resistance (crack stability). The reduced energy consumption of crack propagation in high-speed powder steels was first discovered in reference 7.

The easier fracture of R6M5-OMSP in comparison to R6M5F3-MP after hardening from a temperature of up to 1230°C obviously results from the anisotropy of the structure of the steel: in R6M5-OMSP steel the ratio of austenite grain length to width is approximately 1.1-1.3, whereas in the powder steel this ratio is approximately 1.[8] The easier fracture with elongated grains has been

noted in a number of works.[9] Thus, in the case of R6M5F3-MP after hardening yielding a very small austenite grain (approximately 12 on the scale of GOST 5639-82), superior operational reliability and durability should also be observed. As soon as the austenite grain begins to enlarge, decreasing the length of grain boundaries and increasing both concentration and size of segregations and boundary-area segregations, the propagation of a major crack becomes easier and, in certain cases, is initiated by the large boundary-area particles, which is immediately felt as a significant, up to several times, decrease in impact toughness--fracture of the tool begins to occur primarily by viscous chipping (about 70% at 1230°C and higher, cf. Figure 1). One reflection of the significantly facilitated fracture of R6M5F3-MP steel after bending with hardening is the delamination in the fracture noted above, helping to reduce the operation of fracture due to a decrease in the zone of plastic deformation.

Caption: Figure 2. Microfractogram of fracture in R6M5-OMSP steel after hardening from 1220°C and tempering at 560°C, twice for 1 hour. a. X2400 (fibrous, banded fracture, many pores); b. X8000 (transcrystalline fracture, furrows)

Caption: Figure 3. Microfractogram of fracture of R6M5F3-MP steel after hardening from 1200°C and tempering at 560°C, twice for 1 hour. a. X2400 (equiaxial cup fracture with nonmetallic inclusions); b. X8000 (transcrystalline fracture with areas of intercrystalline fracture, with stream fracture relief on facets)

Caption: Figure 4. Microfractogram of fracture of R6M5F3-MP steel after hardening from 1260°C and tempering at 560°C, twice for 1 hour. a. X10,000 (cracking and delamination of metal); b. X3500 (intercrystalline fracture with brittle crack fracture mechanism)

Still more frequent at present is the practice of selecting the optimal temperature for hardening high-speed powder steel based on bending strength and impact toughness, which are approximately equal to the same characteristics for high-speed steels produced by ordinary metallurgical methods, leading to increased brittleness of the powder tools and low operational reliability. The optimal austenitization temperature of a high-speed powder steel according to the results of our work is the maximum austenitization temperature (to produce maximum red hardness) for which the beginning of austenite grain growth is not observed.

The results of life-cycle testing of m4.5 modulus worm milling cutters of R6M5F3-MP steel (cf. table) fully confirmed this: with the smallest austenite grain growth--from 13(12) to 12(13) according to GOST 5639-82, the mean wear and life of cutters both decrease, and a chip immediately appears on one cutter. A slight further increase in austenitization temperature and corresponding enlargement of austenite grain to No. 12(11-13) causes a very significant decrease in mean tool life and also chips on the cutting elements of the cutters, with the chip on one cutter being so large (on the order of 3 mm) that resharpening was impossible. It should be noted that with identical austenite grain size, additional tempering to decrease hardness by 2-3 HRC

units (mode 2), thus increasing the toughness of the steel, leads to a significant increase in mean tool life and absence of chips.

The low energy consumption of crack propagation in high-speed powder steels is obviously the main reason for the insufficient operating reliability of powder tools when hardened from higher temperatures, and the impossibility of fully utilizing the alloying of the steel, thus justifying its high cost.

Table. Life of m 4.5 Worm Modulus Milling Cutters of R6M5F3-MP* Steel

Mode No.	Hardening temperature **, °C	Austenite grain scale per GOST 5639-82	HRC_e	Life, minutes	Wear, mm	Chipping
1	1175	13(12)	66-67	535; 416	0.5;0.45	No chipping
2	1175 + additional tempering 580°C, 1 h	13(12)	64	526; 503	0.4; 0.3	No chipping
3	1200	13-12	67-68	417; 508	0.45;0.3	Chip on second cutter
4	1220	12(11-13)	68-69	302; 381	0.6; 0.2	Chip on both cutters; 3 mm chip on first cutter

*Tests performed in laboratory of state testing of milling tools of Moscow Tool Plant on Pfauter gear cutter model P630 with continuous adjustment of rotating speed and feed at n = 127 rpm, S_0 = 2 mm/rev, S_M = 6.3-11.5 mm/min, v = 40 m/min working type 45 steel with hardness HV 180-190.
**With subsequent tempering at 560°C, twice for 1 hr.

Conclusions

As a result of studying the microstructure and related fracture surface, it was demonstrated that good operational reliability of tools made of high-speed powder steel type R6M5F3-MP can be achieved due to the specifics of the microstructure of the steel, including absence of anisotropy of austenite grain shape, manifested upon fracture as equiaxial cup fracture, with no fiber or texturing of the fracture, no rough banding, as is characteristic for the fracture of R6M5 steel made by traditional metallurgical method.

References

1. Hellman, P., Hochfeste pulvermetallugische schnellstahle//Industrie—Anzeiger, Vol 102 No 23, 1980, p 18.

2. Fridman, Ya. V., Mekhanicheskiye svoystva metallov [Mechanical Properties of Metals], Vol. 2, Moscow, Mashinostroyeniye Press, 1974.

3. Zelenova, V. D., "Use of Fractography To Estimate Quality of Steel Parts," Kontrol' kachestva termicheskoy obrabotki stalnykh polufabrikatov i detaley: Spravochnik [Quality Control of Heat Treatment of Steel Semifinished Goods and Parts; A Handbook], Moscow, Mashinostroyeniye Press, 1984, p 502.

4. Fonsheyn, N. M., Primeneniye kriteriyev lineynoy mekhaniki razrusheniya v metallovedenii [Use of Linear Fracture Mechanics Criteria in Metal Science], Moscow, Mashinostroyeniye Press, 1979.

5. Romanov, O. N., "Estimating Operational Reliability of Metals and Alloys," Metallovedeniye i term. obrab. metallov, No 12, 1982, p 6.

6. Sokolchuk, K. Yu., Skrynchenko, Yu. M. and Orlov, M. R., "Fracture Toughness and Strength of Powder High-Speed Steels," Metallovedeniye i term. obrab. metallov, No 1, 1988, p 29.

7. Kupaloba, I. K. and Stromenko, O. A., "Microfractographic Study of High-Speed Steel," Zakonomernosti formirovaniya struktury splavov evtekticheskogo tipa [Formation of Structure in Eutectic-Type Alloys], Materials of National Scientific Conference, Dnepropetrovsk, Part 2, 1986, p 28.

8. Almond, E. A. and Irani, R. S., "Relation Between Microstructure and Strength in Conventional and Powder-Processed High-Speed Steels," Powder Metallurgy, No 2, 1981, p 105.

9. Bohmer, M. and Zeigler, G., "Mikrofractorgrafische Untersuchungen zur Beurteilung von Schadenstallen," Prakt. Metallogr., Vol 13, 1976, p 461.

UDC 669.295.548.735.6

Crystal-Chemical Principles in Control of Texture Formation in Titanium Alloy

18420207B Moscow IZVESTIYA AKADEMII NAUK SSSR: SERIYA METALLY No 2, in Russian Mar-Apr 89 (Manuscript received 23 Nov 87) pp 137-40

[Article by A. A. Babareko, Moscow]

[Text] The natural anisotropy of physical-mechanical and chemical, for example corrosion, properties of crystals allows optimization of the usage characteristics of polycrystalline materials by creation of a crystallographic texture.

The nature of natural anisotropy of mechanical properties of metal crystals used for texture hardening of a polycrystal depends on the chemical composition and crystalline structure of the material. For example, the ratio of yield points for HP crystals when compressed along the c and a axes for pure titanium is 2.6, for an alloy of titanium plus 3% Al and 2% Sm-3.2[1] The observed anisotropy results from the fact that alloying of titanium with elements which stabilize the HP phase hardens the crystal more upon twinning deformation, which is primarily active for loading along the c axis, than for deformation by prismatic slipping, which is active for loading along the a axis (the increase in shear stress upon twinning in the system {1122} <1123> from 6.5 to 70, while for prismatic slipping it increases from 2.5 to 20 kg/mm^2. This alloying can increase the normal anisotropy of yield points in compression in sheets with the basic texture to 1.6, which is used to improve the properties of the material in products used under biaxial symmetrical extension.[2] Alloying with elements which stabilize the bcc phase of titanium, in contrast, decreases the natural anisotropy of the mechanical properties of HP-phase crystals. In a pseudo-α alloy in the system Ti-Al-V, the shear stress for prismatic slipping and twinning do not differ by more than 10-15%; therefore, texture hardening in this alloy results primarily from differences in the effective orientation factors for slipping and twinning in a textured sheet.[3] For isometric metals, the orientation factor is the main factor of texture hardening of a polycrystal.

Alloying in the area of a solid solution or with liberation of impurity phases indicates the influence of pressure working and heat treatment of a metal on mechanical texture formation. Suppression of primary twinning by alloying upon deformation in α-titanium alloys can be used to produce a fraction of basic texture reaching 90% by direct rolling. In pseudo-α and (α+β)-titanium alloys, increasing the pressure working temperature can suppress secondary twinning

and rolled products with prismatic texture can be transversely rolled to produce sheets with a fraction of basic texture deflected by not over 25° amounting to 80–90%.

In metals with bcc structure, octahedral texture is used for texture hardening of products used with biaxial deformation and to improve the forging properties of sheets. The development of the {111} <hhkl> texture in the β-phase of titanium alloys, which is a solid solution based on the bcc structure, depends on the degree of alloying. In hot-rolled pseudo-α class alloys with low content of alloying elements stabilized by the β-phase, the plane deformation {001} <110> texture is primarily developed, whereas in (α+β) titanium alloys a mixed β-phase texture is formed, while in pseudo-α class alloys the octahedral texture predominates. The regular change in deformation texture of the bcc phase of titanium with increasing content of elements stabilizing the β-phase can be related to the influence of alloying on the crystallographic mechanism of plastic flow, namely with decreasing dislocation mobility with the Burgers vector *a* <100>, forming the texture of plane deformation {001} <100>.

For titanium-group-metal alloys which have phase transitions in the temperature interval of metalworking, texture formation also depends on the following factors. Formation of the texture of the low-temperature HP phase is determined both by the process of texture formation in the high-temperature bcc phase, and the bcc → HP conversion, deformation and heat treatment of the HP phase. The converted phase is represented by a complex hierarchy of structure elements. We must distinguish for it between intragrain texture, within the limits of the matrix β-grain and texture averaged through the volume of the material. Deformation at temperatures above the equilibrium transition point T_t of the equilibrium (α+β) → β transition causes deformation of the β-phase deformation texture with some set of components in the area of orientation {001}-{111} <110> and {111} <112>. Upon cooling from the deformation temperature within each matrix grain a multicomponent α-phase texture is formed, resulting from the multivariant oriented phase transition $\beta \rightarrow \alpha$. With heat and plastic working of alloys in the temperature interval of the martensite transition upon deformation single-component textures arise within the matrix grains. Their development results from the preference of those orientation versions of the shear transformation which make the greatest deformation of the conversion, corresponding to macrodeformation of the product under the influence of external applied stresses. If the texture of the matrix phase has one component, the texture of the converted phase in the entire volume of the material also has one component. With multicomponent texture of the matrix phase, the converted phase has one-component texture within the matrix grain, but multicomponent texture throughout the volume of the material.

The development of models of shear conversions $\beta \rightarrow \alpha'$, $\beta \rightarrow \alpha''$ in alloys based on titanium-group metals with determination of the crystallographic shear systems upon conversions has allowed computation of the orientation of single-version martensitic transitions upon pressure working. This was done on the basis of analysis of conversion deformation tensors.[4] Figure 1 shows the calculated reverse band figures of the three main sheet directions. For metal with different initial ideal β-phase textures against the background of

multivariant $\beta \rightarrow \alpha$ conversion textures, orientations are denoted which are formed in the process of single-version martensite conversion during rolling.

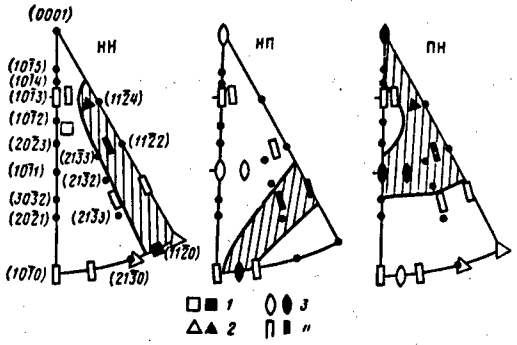

Figure 1. Reverse Band Figures of Main Directions of the Sheet Normal Stress (left), Rolling Direction (middle) and Transverse Direction (right), Designed for Multivariant Phase $\beta \rightarrow \alpha$ Conversion Texture Upon Cooling of Metal From the Rolling Temperature and for 1-Version Martensite Transition During Rolling (marked by dark blocks); β-Phase Initial Texture Axes
1. <100>; 2. <111>; 3. <110>; 4. <112>

Deformation of alloys in the temperature interval A_d^n-M_d^n where A_d^n is the temperature at which the reverse martensite conversion begins upon deformation, which is dependent on the orientation of the converted phase with compression significantly greater than the conversion deformation, is accompanied by cyclical processes of texture and phase conversions. These conversions include direct and reverse martensite conversions and deformation of both phases, improving their texture. Let us study rolling in this temperature interval of an alloy in the system Ti-Al-V, the β-phase deformation texture of which contains the most stable orientation {001} <110>.

According to the calculations of reference 4 upon martensitic $\beta \rightarrow \alpha'$ conversion by homogeneous shift in the systems {334} <446> and {556} <334>, the material with the matrix texture experiences plane deformation with 10% compression in the direction perpendicular to the rolling plane and 10% extension in the direction of rolling. This is the entire conversion deformation of the volume of the material. As the degree of compression increases still further upon rolling the phase conversion having prismatic orientation $\{5\bar{2}30\}\ \langle\bar{1}8\bar{7}0\rangle$ changes its texture to $\{2\bar{1}\bar{1}0\}\ \langle 01\bar{1}0\rangle$ in the process of deformation of the α phase by prismatic slipping. Based on a geometric interpretation of slipping deformation according to Boas and Schmidt, this reorientation corresponds to axial compression upon rolling of about 15%. When this position is reached according to deformation tensor analysis, the reverse martensite transition $\alpha\ \{2\bar{1}\bar{1}0\}\ \langle 01\bar{1}0\rangle \rightarrow \beta\ \{111\}\ \langle 11\bar{2}\rangle$ occurs, accompanied by conversion deformation with axial compression in the normal direction and rolling direction by 4%. Since in the β-phase of the alloy the {001} <110> rolling texture is stable, further deformation of the β martensite leads to a change in its orientation in the process of deformation by slipping and twinning.

When the stable {001} <110> texture is reached, the entire cycle of phase and texture transitions may be repeated (Figure 2).

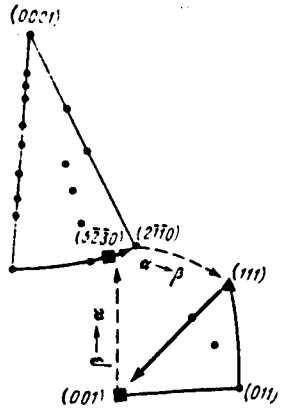

Figure 2. Diagram of Cyclical Processes of Texture and Phase Transitions Upon Rolling of Alloys in System Ti-Al-V in Temperature Interval of Martensitic Transition Upon Deformation

Deformation of alloys at temperatures below A_d^n eliminates the reverse martensite conversion upon deformation and leads to development of a rolling texture of the low-temperature phase of deflected basis and basis type.

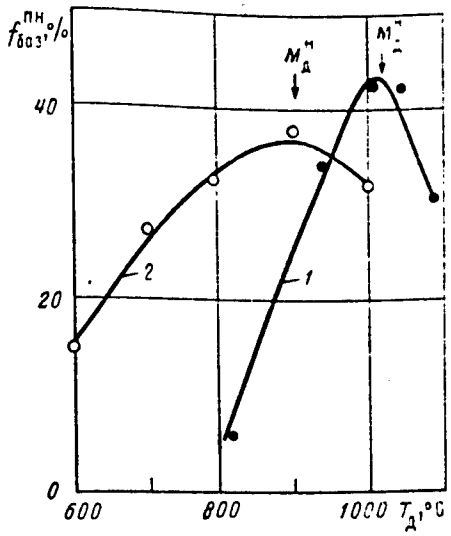

Figure 3. Estimate of Temperature M_d^n of Beginning of Martensite Conversion Upon Deformation of Titanium Alloys Based on Nonmonotonic Change in Rolling Texture as a Function of Deformation Temperature

1. Pseudo-α alloy in system Ti-Al-V; 2x (α + β) alloy f_{baz}^{PN} fraction of basis texture in transverse direction of sheet

The temperature of martensitic conversions upon deformation depends on the chemical composition of the alloys (Figure 3). With constant composition in

the Ti–Al–V system alloy, the nature of the rolling temperature is used to invoke the structural sequence of the temperature of martensitic conversion upon rolling (Figure 4). Using it, one can widely vary the alloy processing temperature in order to form textures of a certain type with varying anisotropy of properties.

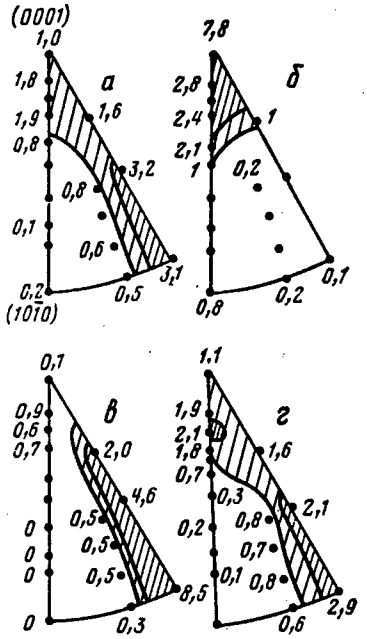

Figure 4. Influence of High-Temperature Intermediate Annealing of Rolled Product on Development of Rolling Texture of Alloy in System Ti–Al–V at T_d = 950 (a,c), 820 (b) and 700°C (d)
a,b. Annealing of blanks for 1 hr at 1000°C; c,d. No annealing of blanks

Conclusions

1. The development of the plane deformation texture in titanium α alloys depends on the degree of alloying with elements which stabilize the α–phase and the deformation temperature. Formation of the basic texture, yielding the maximum normal anisotropy of the material, is stimulated by increasing the degree of alloying and increasing the α–phase deformation temperature.

2. The relationship of plane deformation texture components in the β–phase of titanium is determined by the degree of its alloying with elements which stabilize this phase. In titanium pseudo–β alloys, an octahedral plane deformation texture is formed, whereas in pseudo–α alloys deformed in the area of temperatures where the β phase exists the {001} <110> texture is formed and for (α+β) alloys developed of a mixed–type β–phase texture is characteristic.

3. Upon deformation of pseudo–α and (α+β) titanium alloys in the temperature area between M_d^n and A_d^n, a single–version $\beta \rightarrow \alpha$ phase–transition texture is formed. The development of a prismatic {1120} <1100> component in this texture is clearer, the more perfect the β–phase of the alloy the {001} <110> texture is.

For alloys of these classes deformed at temperatures above the transition temperature T_t, it is characteristic that a multivariant phase transition α-phase texture develops with pyramidal and prismatic components, while for deformation at temperatures below A_d^n the texture of deformation of the α-phase develops.

References

1. Ageev, N. V., Rubina, E. B., and Babareko, A. A., "The Influence of Deformation Mechanism on Yielding Characteristics in α-Single Crystal of Ti-Al-Sn α-Alloy," Titanium-80: Proc. of the IV Intern. Conf. on Titanium, Kyoto, Japan, 1980, Vol 2, Kyoto, 1981, p 887.

2. Babareko, A. A., "Texture in Metals and Alloys," Itogi nauki i tekhniki. Ser. Metallovedeniye i term. obrabotka [Results of Science and Technology. Metal Science and Heat Treatment Series], Vol 13, 1980, p 79.

3. Babareko, A. A. and Egiz, I. V., "Construction of Yield Surfaces of Metallic Materials with Single-Component Textures," Izv. AN SSSR. Metally, No 2, 1985, p 125.

4. Babareko, A. A. and Belova, O. S., "Study of Phase Transition in Titanium Alloys upon Deformation," Fizika metallov i metallovedeniye, Vol 62 No 5, 1986, p 944.

UDC 621.979.003.1

Ensuring Efficiency of Heavy, One-of-a-Kind Die Forging Equipment

907D0076b Moscow KUZNECHNO-SHTAMPOVOCHNOYE PROIZVODSTVO in Russian No 11, Nov 89 pp 3-5

[Article by A. P. Kovalev, N. V. Kovalev: "Ensuring the Efficiency of Heavy and One-of-a-Kind Die Forging Equipment"]

[Text] An important direction in ensuring the efficiency of heavy and one-of-a-kind die forging equipment (DFE) is the integrated feasibility analysis (FA) of design approaches which provides the correct orientation for the development of economically sound requirements for the technical parameters of future articles, demonstrates the most effective direction in improving quality and technical level, serves as a tool for evaluating alternatives and selecting economical designs, and provides standard data for subsequent development.

When new die forging equipment is being developed, this is achieved by defining the economically sound main characteristics for forging equipment (technological cycle, capacity, material consumption, etc.) and the organizational procedures that regulate the scheduling, record-keeping and monitoring the achievement of technical and economic indicators (TEI) for this equipment.

An urgent task in design is the selection of economically justified individual engineering, production, and operating parameters and indicators, since a change in any of them causes not only to savings, but also specific costs.

One of the basic characteristics of the yield of equipment operating in automatic mode is the technological cycle. Shortening the technological cycle increases equipment capacity, but at the same time causes a certain increase in expenditures for the use of faster mechanisms, high-speed drives, automation devices, and control systems.

Efficient use of automation devices in automated forging complexes (AFC) requires a reduction in the overall annual costs of operating AFC over those for manually operated DFE:

$$C_m+E_nK_m(N_a/N_m)>C_a+E_nK_a, \quad (1)$$

where C_m, C_a are the technological prime cost of manufacturing the annual

output of forged pieces with manually operated equipment and AFC, adjusted to the output corresponding to AFC capacity, rubles; E_n, a normalizing factor for the efficiency of capital investment; K_m, K_a, capital investments by the producer for the two alternatives, rubles; N_m, N_a, the equipment's annual production capacity, pc/yr.

Formula (1) is used to calculate variable expenditures. Therefore, the technological prime cost of forged blanks must include costs related to running the equipment and the wages of basic workers. These expenditures may be calculated using standard operating expenses per unit of operating time:

$$C_{ma}=i_{ma}i_{aa}t_{ma}N_a+pK_{ma}, \quad (2)$$

where i_{ma}, i_{aa} are operating expenses to run manual equipment and equipment outfitted with automation devices per unit of time, ruble/sec; t_m, t_a, the technological cycles for these alternatives, sec; p, renovation depreciation rate.

Using $K_m=P_m$, $K_a=P_a$ (P_m and P_a are equipment prices), after substituting (2) into inequality (1) and transforming it, we obtain

$$t_a<(i_m/i_a)(t_m) + [(p+E_n)/(i_aN_a)][P_m(N_a/N_m)-P_a). \quad (3)$$

By calculating prices for new machine building products for manufacturing purposes with the State Committee on Pricing's procedure (Footnote)("Metodika opredeleniya optovykh tsen na novuyu mashinostroitelnuyu produktsiyu proizvodstvenno-tekhnicheskogo naznacheniya (vremennaya) [Procedure for Determining Wholesale Prices for New Machine Building Equipment for Manufacturing Purposes], approved by resolution of the USSR State Committee on Pricing of 30 October 1987, No. 760. Moscow, "Preyskurant", 1987, 29 pp), we established the mandatory reduction in prices per unit of useful effect, which denotes the need to meet the condition $P_m(N_a/N_m)\geq P_a$.

Thus the second term in the first half of inequality (3) is either positive or zero. In the second case, which provides for the limit price, equation (3) takes the form $t_a<(i_m/i_a)t_m$.

Determining the cost-effective technological cycle requires the following normalizing condition: automated equipment must ensure a minimum 15 percent reduction in overall costs. Then the expression for the limit efficient cycle will take the form

$$t_{ae}=0.85(i_m/i_a)t_m) + (p+E_n)/i_aN_a)[0.85P_m(N_a/N_m)-P_a. \quad (4)$$

If $P_m(N_a/N_m)=P_a$, we derive the equation

$$t_{ae}=0.85(i_m/i_a)t_m) - 0.15(p+E_n)P_a/i_aN_a) \quad (5)$$

Equation (5) can be used to calculate efficient AFC technological cycles with different degrees of automation depending on the cost of the equipment and the weight of the pieces in large-series and mass forging.

The patterns of the change in the efficient forging cycle when 25-MN hot forging crank presses are automated illustrate the need to consider this factor in practical work to formulate the technical requirements for equipment at the early stages of its development.

Figure 2 [not illustrated] presents the flow chart for the subsystem controlling the economy of new equipment at a DFE production enterprise.

The level on which the EFA is organized must be increased by the use of a set of documents guiding, regulating, and coordinating the work of individual enterprise subdivisions and services involved in the economy control process. An example of a list of instructions for ensuring the economy of new equipment in a DFE production association is shown in the table.

Document	Application
Controlling the Economy of New Equipment. Basic Regulations.	Process of EFA for New Equipment at the Development Stage.
Planning the Technical and Economic Indicators of New Equipment.	Procedure for Determining the Technical and Economic Indicators of New Equipment at the Pre-Design Stages
Organization of Planning, Rate-Setting, Record-Keeping, and Control of Design Work.	System for Planning, Rate-Setting, Record-Keeping, and Controlling Design Work.
Procedure for the Development of a Feasibility Study for Few Die Forging Equipment at the Design Stage.	Organization of Work on a Feasibility Study for New Equipment at the Design Stages
Organization of Efforts toward Material Incentives for New Equipment Development.	System of Material Incentives for New Equipment Developers.
Organization of Efforts to Study the Technical and Economic Indicators of Equipment Operation.	Organization of the Study of Economic Indicators for Equipment Operation

An enterprise standard "Controlling the Economy of New Equipment. Basic Regulations" was introduced within the framework of the integrated system for increasing production efficiency and work quality at the Voronezh "Tyazhmekhpress" PO [Production Association]. There is another standard "Planning the Technical-Economic Indicators of New Equipment" which establishes the procedure for planning the TEIs of new die forging equipment during pre-design technical and economic research. The standard stipulates that TEIs for equipment are to be planned to reflect its technical and economic level and provide a comprehensive description of the equipment as an

object of design, production, and operation; a coefficient for the increase in equipment capacity compared to what it is replacing; the design labor consumption to manufacture the equipment; limit price; prime cost of goods; and annual economic effect.

TEIs are planned by doing the following work: analyzing the indicators of current production, determining the level of planned TEIs for new equipment, analysis, evaluation, and development of recommendations on achieving the required level of TEI for the equipment; filling in charts of planned TEIs, and step-by-step control of their achievement.

The level of regulated TEIs must be at least that established by state and branch standards and specific comprehensive programs in effect in the industry. The regulation of design TEIs orients developers to increase the efficiency and quality of developments and create new equipment with high economy.

To check the results and take immediate steps at the development stages, the enterprise introduced the enterprise standard "Procedure for Developing the Feasibility Study for New Die Forging Equipment at the Design Stage." In addition to basic TEIs at the design stage, additional indicators, including specific material consumption and energy consumption are checked. These are compared to the indicators of the best domestic and foreign products; for universal presses, with the TEIs recommended by standards on the basis of parameters and dimensions.

The development of new DFE for individual and small-series production includes several FA cycles at the research and experimental design stages: pre-design research, development of specifications, request for proposals, preliminary and detail designs, and contractor documentation. Each FA cycle includes the following operations: developing a file of raw data, developing mathematical economic models, calculation and analysis of TEIs, and revising designs on the basis of FA data.

In this structure for the FA of DFE design approaches, pre-design economic studies are considered a separate stage preceding the development of the specifications. The end result of the work at this stage is the development of the limit level of basic TEIs for the equipment.

Regulation of limit TEI values and limits for resource consumption, as well as control of their achievement on the basis of rational FA organizational procedures ensures a high level of economic developments, objective evaluation of the labor of design services serves as the basis for improving the system for stimulating and organization the enterprises' self-supporting activity.

Experience working to ensure the economy of new equipment has confirmed its high effectiveness, which is achieved by increasing the quality and scientific procedural level of the FA for the equipment and, ultimately, by conserving resources and increasing the yield during the development, production, and operation of die forging equipment.

- END -

22161
57

NTIS
ATTN: PROCESS 103
5285 PORT ROYAL RD
SPRINGFIELD, VA 22161

Foreign Broadcast Information Service (FBIS) and Joint Publications Research Service (JPRS) publications contain political, military, economic, environmental, and sociological news, commentary, and other information, as well as scientific and technical data and reports. All information has been obtained from foreign radio and television broadcasts, news agency transmissions, newspapers, books, and periodicals. Items generally are processed from the first or best available sources. It should not be inferred that they have been disseminated only in the medium, in the language, or to the area indicated. Items from foreign language sources are translated; those from English-language sources are transcribed. Except for excluding certain diacritics, FBIS renders personal names and place-names in accordance with the romanization systems approved for U.S. Government publications by the U.S. Board of Geographic Names.

Headlines, editorial reports, and material enclosed in brackets [ ] are supplied by FBIS/JPRS. Processing indicators such as [Text] or [Excerpts] in the first line of each item indicate how the information was processed from the original. Unfamiliar names rendered phonetically are enclosed in parentheses. Words or names preceded by a question mark and enclosed in parentheses were not clear from the original source but have been supplied as appropriate to the context. Other unattributed parenthetical notes within the body of an item originate with the source. Times within items are as given by the source. Passages in boldface or italics are as published.

SUBSCRIPTION/PROCUREMENT INFORMATION

The FBIS DAILY REPORT contains current news and information and is published Monday through Friday in eight volumes: China, East Europe, Soviet Union, East Asia, Near East & South Asia, Sub-Saharan Africa, Latin America, and West Europe. Supplements to the DAILY REPORTs may also be available periodically and will be distributed to regular DAILY REPORT subscribers. JPRS publications, which include approximately 50 regional, worldwide, and topical reports, generally contain less time-sensitive information and are published periodically.

Current DAILY REPORTs and JPRS publications are listed in *Government Reports Announcements* issued semimonthly by the National Technical Information Service (NTIS), 5285 Port Royal Road, Springfield, Virginia 22161 and the *Monthly Catalog of U.S. Government Publications* issued by the Superintendent of Documents, U.S. Government Printing Office, Washington, D.C. 20402.

The public may subscribe to either hardcover or microfiche versions of the DAILY REPORTs and JPRS publications through NTIS at the above address or by calling (703) 487-4630. Subscription rates will be provided by NTIS upon request. Subscriptions are available outside the United States from NTIS or appointed foreign dealers. New subscribers should expect a 30-day delay in receipt of the first issue.

U.S. Government offices may obtain subscriptions to the DAILY REPORTs or JPRS publications (hardcover or microfiche) at no charge through their sponsoring organizations. For additional information or assistance, call FBIS, (202) 338-6735,or write to P.O. Box 2604, Washington, D.C. 20013. Department of Defense consumers are required to submit requests through appropriate command validation channels to DIA, RTS-2C, Washington, D.C. 20301. (Telephone: (202) 373-3771, Autovon: 243-3771.)

Back issues or single copies of the DAILY REPORTs and JPRS publications are not available. Both the DAILY REPORTs and the JPRS publications are on file for public reference at the Library of Congress and at many Federal Depository Libraries. Reference copies may also be seen at many public and university libraries throughout the United States.